



A novel Zeonex based oligoporous-core photonic crystal fiber for polarization preserving terahertz applications

Md. Saiful Islam^{a,*}, Jakeya Sultana^{a,b}, Alex Dinovitser^a, Brian W.-H. Ng^a, Derek Abbott^a

^a School of Electrical & Electronic Engineering, The University of Adelaide, SA 5005, Australia

^b Department of Electrical & Electronic Engineering, Islamic University of Technology, Gazipur 1704, Bangladesh

ARTICLE INFO

Keywords:

Photonic crystal fiber
Birefringence
Dispersion
Waveguide
Effective material loss
Terahertz

ABSTRACT

A novel waveguide consisting of oligo-porous core photonic crystal fiber (PCF) with a kagome lattice cladding has been designed for highly birefringent and near zero dispersion flattened applications of terahertz waves. The wave guiding properties of the designed PCF including birefringence, dispersion, effective material loss (EML), core power fraction, confinement loss, and modal effective area are investigated using a full vector Finite Element Method (FEM) with Perfectly Matched Layer (PML) absorbing boundary condition. Simulation results demonstrate that an ultra-high birefringence of 0.079, low EML of 0.05 cm⁻¹, higher core power fraction of 44% and negligible confinement loss of 7.24×10^{-7} cm⁻¹ can be achieved at 1 THz. Furthermore, for the y-polarization mode a near zero flattened dispersion of 0.49 ± 0.05 ps/THz/cm is achieved within a broad frequency range of 0.8–1.7 THz. The fabrication of the proposed fiber is feasible using the existing fabrication technology. Due to favorable wave-guiding properties, the proposed fiber has potential for terahertz imaging, sensing and polarization maintaining applications in the terahertz frequency range.

© 2018 Elsevier B.V. All rights reserved.

1. Introduction

In the electromagnetic frequency spectrum, the 0.1–10 THz frequency range is commonly known as the terahertz band [1]. The terahertz band bridges the gap between the microwave and infrared frequencies making it a potential candidate for applications in the field of sensing [2,3], pharmaceutical drug testing [4], spectroscopy [5–7], biomedical engineering [8], DNA hybridization detection and biotechnologies [9] and so on. Devices such as terahertz couplers [10], splitters [11] and gratings [12,13] are also attracting significant attention. Emerging terahertz applications require highly birefringent, dispersion flattened and low loss terahertz waveguides [14,15]. The main function of waveguides is to transmit electromagnetic waves as well as information with near zero dispersion [16]. Over the last decade, a number of waveguide structures in the terahertz regime have been designed and studied for efficient and reliable transmission of terahertz waves. Firstly, electromagnetic waves in the terahertz spectrum were guided by metallic waveguides [17]. There are various types of metallic waveguide such as metallic circular wave guide [18], parallel plate waveguide [19], bare metal wire [20] and slit waveguides [21]. In metallic waveguides terahertz pulses face a number of problems. For example, Ohmic losses occur due to metal strips, dielectric losses occur

in the substrate of circular metallic waveguides, divergence losses in parallel plate waveguides occur due to beam spreading in the unguided medium, radiative losses in bare metallic waveguide occurs due to weak confinement of the mode to the structure and attenuation loss occurs due to larger metal area of the metallic slotted waveguide. Another key waveguide for the terahertz regime is a fiber dielectric waveguide. These terahertz fibers can have either (i) a solid core, (ii) a hollow core, or (iii) porous core. In a hollow core fiber, terahertz waves are limited to a short propagation distance. Furthermore, the bending losses are significant as they are inversely proportional to the diameter and bending radius of the fiber. These deleterious features have slowed down the acceptance of hollow core waveguides and restricted their use today to applications in chemical sensing, thermometry, and laser power delivery [22–25]. Solid core fibers were also proposed earlier but disregarded due to their higher material absorption loss as the core is based on solid material.

Porous core photonic crystal fiber [26–30] have attracted significant interest due to the ability to readily determine optical properties through design, due to their dependence on geometric features. In a PCF, the designer can control the structure by adjusting the number of air holes, the air hole diameter, pitch size, core radius etc. In a PCF, the birefringence is one or two orders greater than conventional polarization

* Corresponding author.

E-mail address: mrsaiful.islam@adelaide.edu.au (Md.S. Islam).

maintaining terahertz fibers that can be achieved by introducing an anisotropic structure both in the core and cladding regions [31].

Several types of highly birefringent and low loss terahertz PCFs were proposed earlier for the purpose of polarization maintaining terahertz applications. In 2008, Atakaramians et al. proposed a porous core PCF for polarization maintaining applications of terahertz waves [32]. Using asymmetrical sub-wavelength air-holes within the core they obtained a low birefringence of 0.026. Later, to obtain a high birefringence Chen et al. proposed a super cell structure but failed to increase the birefringence [33]. In 2015, a slotted core photonic crystal fiber was proposed by Raonaqul [34] et al. They showed a higher birefringence of 0.075 but failed to reduce the loss and flatten the dispersion properties. Later, a dual air hole unit based PCF [35] was proposed obtaining a moderate birefringence of 0.033 with a low EML of 0.043 dB/cm. However, the dispersion properties of their proposed dual air hole unit based fiber was not reported. Next, to improve the birefringence and reduce the EML with improved flattening of the dispersion, Hasan and coworkers [36] proposed a new type of polarization maintaining spiral PCF. They were able to increase the birefringence to 0.0483 but with a higher value of EML of 0.085 cm^{-1} with higher dispersion variation of 0.97 ps/THz/cm in the x -polarization mode and 1.42 ps/THz/cm in the y -polarization mode. A dual asymmetrical terahertz PCF [37] with a birefringence of 0.045 was then proposed. Recently, a new type of PCF named the oligo-porous core PCF was proposed by Wu and coworkers [31]. They obtained a birefringence value of 0.03 with a high value of EML of 20%–40% using Topas as the bulk material. The same research group then proposed a triple-hole core [38] based PCF and obtained a birefringence value of the order of 10^{-2} with a higher EML value of 0.07 cm^{-1} . Moreover, an elliptical air hole based hexagonal structure in the core surrounded by a circular air hole based hexagonal cladding was proposed by Ahmed [39] et al. They obtained a lower value of birefringence of 0.0119 and higher value of EML of 0.0689 cm^{-1} . So, from the discussed literature review of terahertz PCF it can be concluded that there is scope for PCF improvement in terms of birefringence, dispersion, and loss etc. In practice, the trade-offs between high birefringence, flattened dispersion, low loss, high power confinement and low confinement loss based terahertz fiber are challenging.

In this context, we propose a new type of Zeonex based terahertz photonic crystal fiber named oligo-porous core fiber using elliptical structured air holes in the core surrounded by kagome cladding. Several types of core structure [40–43] inside a kagome cladding have been proposed earlier but to the best of our knowledge an oligo-porous core structure inside a kagome cladding has not been proposed for terahertz wave propagation. The anisotropic structure of elliptical air holes inside the core simultaneously offers high birefringence and low effective material loss. Furthermore, the compact geometry of the kagome cladding directs most of the useful power throughout the core region. The fabrication of the PCF is readily possible using the existing fabrication techniques. We anticipate that the fiber will have applications in the fields of polarization maintaining transmission systems and dispersion compensation applications.

2. Modeling of the proposed terahertz PCF

Fig. 1 shows the full cross sectional view of the proposed oligo-porous core PCF. We used kagome lattice structure because it offers a very low confinement loss in a broad frequency range [43]. The core is designed using three elliptical air holes to enhance the asymmetry between the polarization modes. The elliptical air-hole arrangements in the core can be structured as dual-hole, triple-hole or other anisotropic structures, and are referred to as oligo-porous cores [31].

In Fig. 1 the symbol D_{core} denotes the length of the core which is twice the circumradius of the hexagon. Also, L and L_1 denote the major axis length of center ellipse and ellipses either side of the center ellipse respectively. It is well known that, during standard fabrication $\pm 2\%$

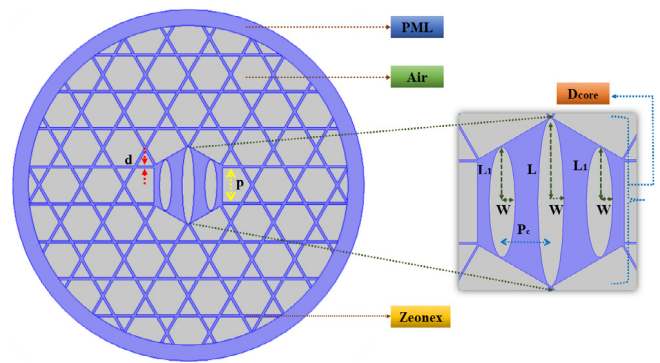


Fig. 1. Cross section of the proposed kagome lattice PCF.

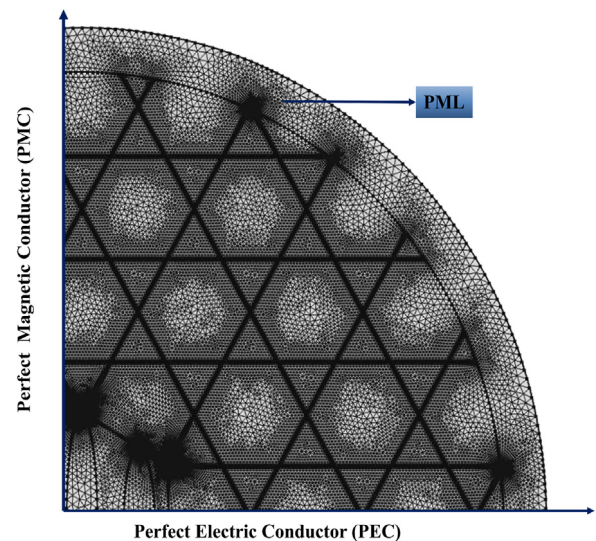


Fig. 2. FEM mesh and boundary conditions for characteristic computation of the proposed Zeonex based PCF.

variation in global parameters of a PCF can occur [3] and considering that fact we choose a maximum major axis length of $L = 0.49D_{\text{core}}$ and $L_1 = 0.32D_{\text{core}}$ respectively. Here, W indicates the length of minor axis of each elliptical air holes and considering the fabrication fact the maximum possible value of W is $0.143D_{\text{core}}$. The center to center distance between the elliptical air holes is denoted by P_c whose maximum value of $P_c = 0.205D_{\text{core}}$. Further reduction of P_c may result in overlap of the air holes with one another and that may create fabrication difficulties. In the cladding region the distance between parallel struts is defined by P which changes with D_{core} whereas the strut width is defined as d .

There are several polymer materials such as PMMA, Teflon, Silica, Topas and Zeonex that can be used as the background material of a terahertz PCF. Among them Cyclo Olefin Polymer (COP) commercially known as Zeonex is used as the base material of the proposed fiber because of its flat refractive index at terahertz, lower bulk absorption loss (0.2 cm^{-1} at terahertz range), low water absorption, high transparency, high glass transition temperature and excellent optical stability after humidity and heat exposure [44–46].

Commercially available software COMSOL v4.3b is used for designing the structure and simulating the result. A finite element method is used to calculate the modal characteristics of the fiber. To improve the accuracy of calculation using COMSOL we used *extremely fine* mesh element to characterize the PCF. The elements and boundary conditions for an *extremely fine* mesh is shown in Fig. 2. During simulation the

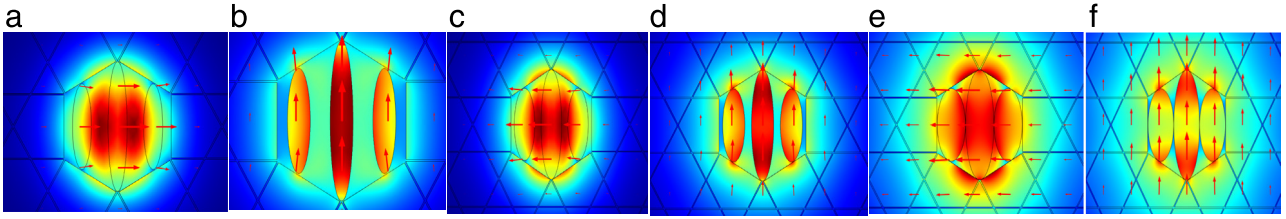


Fig. 3. E-field distribution for (a) $W = 27 \mu\text{m}$, x-pol (b) $W = 27 \mu\text{m}$, y-pol (c) $W = 38.5 \mu\text{m}$, x-pol (d) $W = 38.5 \mu\text{m}$, y-pol (e) $W = 50 \mu\text{m}$, x-pol (f) $W = 50 \mu\text{m}$, y-pol.

average element quality obtained from the Comsol software was 0.90% that indicates less than 0.1% computational error. A perfectly matched layer absorbing boundary condition of radius 10% to the total fiber radius is applied outside of the computational region to strongly absorb outgoing waves from the interior. The inner radius of the PML boundary is $737.77 \mu\text{m}$. The total fiber diameter is approximately $1622 \mu\text{m}$.

Birefringence is an optical property of a PCF having a refractive index that depends on the polarization and propagation direction of light. For a fiber to be operated as an effective polarization maintaining terahertz PCF, the level of birefringence should be as high as possible. Keeping this in mind, we first investigated the level of birefringence in the fiber. It can be calculated by the following equation [26],

$$B = |n_x - n_y| \quad (1)$$

where, n_x and n_y indicates the effective refractive index of the x and y polarization mode respectively.

Propagation of terahertz waves through an optical fiber mostly suffers from effective material loss or material absorption loss. Note that EML is the major loss mechanism of a fiber that can be calculated by the following expression [28],

$$\alpha_{\text{eff}} = \sqrt{\frac{\epsilon_0}{\mu_0}} \left(\frac{\int_{\text{mat}} n_{\text{mat}} |E|^2 \alpha_{\text{mat}} dA}{|\int_{\text{all}} S_z dA|} \right) \quad (2)$$

here, n_{mat} is the refractive index and α_{mat} is the bulk material absorption loss of Zeonex, ϵ_0 is the permittivity and μ_0 is the permeability of free space [32,35,37], S_z is the z -component of the Poynting vector $S_z = \frac{1}{2}(E \times H^*)z$ where, E is the electric field and H^* indicates the complex conjugate of the magnetic field component.

Another important parameter to be considered for a PCF is its confinement loss. It depends upon the core porosity and number of rings used in the cladding. It can be calculated by the following equation [26],

$$L_c = \left(\frac{4\pi f}{c} \right) \text{Im}(n_{\text{eff}}), \text{cm}^{-1} \quad (3)$$

where, $\text{Im}(n_{\text{eff}})$ represents the imaginary part of the complex refractive index and f is the operating frequency.

Next, we consider the power flow distribution in different regions of the proposed fiber. The power fraction of a PCF can be calculated by [30],

$$\eta' = \frac{\int_X S_z dA}{\int_{\text{all}} S_z dA'} \quad (4)$$

where X represents the core region, the cladding region or the material region. In our proposed PCF we calculated the amount of useful power transmitted through the core region.

Dispersion is also an important wave-guiding property to be considered in a PCF design because it determines the amount of pulse spreading when the light pulses are transmitted through an optical fiber. The dispersion property of a fiber can be calculated by [27],

$$\beta_2 = \frac{2}{c} \frac{dn_{\text{eff}}}{d\omega} + \frac{\omega}{c} \frac{d^2 n_{\text{eff}}}{d\omega^2}, \text{ps}^2/\text{THz}/\text{cm} \quad (5)$$

where, ω is the angular frequency and c is the speed of light.

The modal effective area is also an important parameter of interest to be considered for a PCF design. Higher values of effective area lead to

useful applications in laser and communication devices while PCF with lower values of effective area is useful for nonlinear effects. The modal effective area of a fiber can be calculated by [30],

$$A_{\text{eff}} = \frac{[\int I(r) r dr]^2}{[\int I^2(r) r dr]^2} \quad (6)$$

where, $I(r) = |E_t|^2$ is the electric field of the fundamental guided mode.

Finally, it is important to explore the fabrication possibilities for the PCF. The proposed waveguide consists of a kagome structure in the cladding and elliptical air hole structure in the core. Kagome lattice PCF with a different complex core structure has already been fabricated by a research group at the Max Planck Institute [47]. Another technique based on extrusion [48] allows fabrication of almost all types of PCF and this can achieve elliptical [49] air holes inside the core. Moreover, fibers with elliptical shaped air holes have already been fabricated in Refs. [50,51]. In addition, for the manufacture of extrusion dies the 3D printing technology paves the way to fabricate the highly asymmetric air holes including elliptical air holes [52]. Therefore, with recent advances in existing fabrication techniques, the proposed PCF can be potentially fabricated.

3. Results and discussion

The mode field distribution of the proposed PCF at 1 THz, 350 μm core length, different ellipse width (W) and orthogonal polarization modes is shown in Fig. 3. It is confirmed that light is well confined in the porous core region and it can be seen that light confinement in x and y polarization mode is different. This is because of the asymmetrical shaped elliptical air holes used in the core. So, it can be assumed that there can be other modes present in the fiber than the single mode but for the other modes light will be propagated outside the core area. Therefore when a pulse of light will emerge at the center of the fiber only the fundamental modes will be propagated through the core region [3]

The characteristics of birefringence and EML with respect to different values of D_{core} are shown in Fig. 4. It can be seen that birefringence increases with D_{core} increase and maximum birefringence is obtained at 400 μm . The reason is that as D_{core} increases the index difference between core and cladding increases. It can also be seen that EML increases with D_{core} because of increased amount of background material inside the core. It is seen that lowest amount of EML is obtained at 300 μm and y -polarization mode. Therefore we choose y -polarization mode as optimum. However, we cannot choose 300 μm as optimum because at that point the birefringence is lowest. Therefore, considering both the characteristics of birefringence and EML we choose 350 μm as optimum design parameter where the EML is 0.05 cm^{-1} and value of birefringence is 0.079.

At different elliptical air hole width Fig. 5 demonstrates the variation of birefringence with respect to frequency. It clearly demonstrates that higher W values reduce the birefringence. This is because, as the value of W increases some of the useful power starts to spread outside the core and thus the index contrast between the x and y polarization modes decreases. It is necessary to mention that the minor axis length $W = 0.143 D_{\text{core}}$, $W = 0.11 D_{\text{core}}$ and $W = 0.077 D_{\text{core}}$ corresponds to 27 μm , 38.5 μm , and 50 μm respectively.

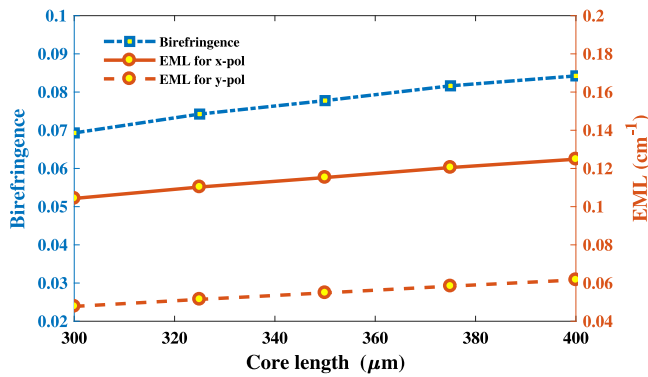


Fig. 4. Birefringence and EML with respect to different D_{core} , 1 THz, $d = 4 \mu\text{m}$ and $W = 27 \mu\text{m}$.

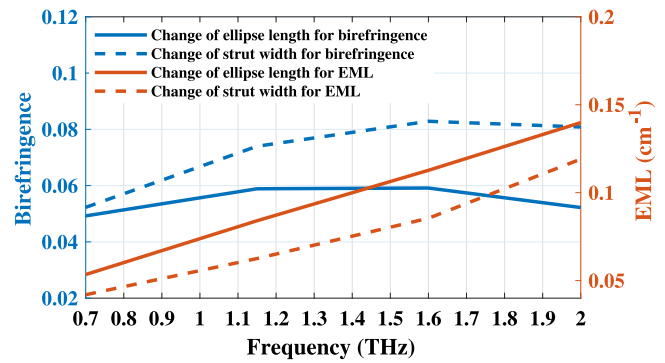


Fig. 6. Birefringence and EML vs frequency at optimal D_{core} , with $d = 8 \mu\text{m}$, $L = 0.43D_{core}$, $L_1 = 0.26D_{core}$ and $W = 0.077D_{core}$.

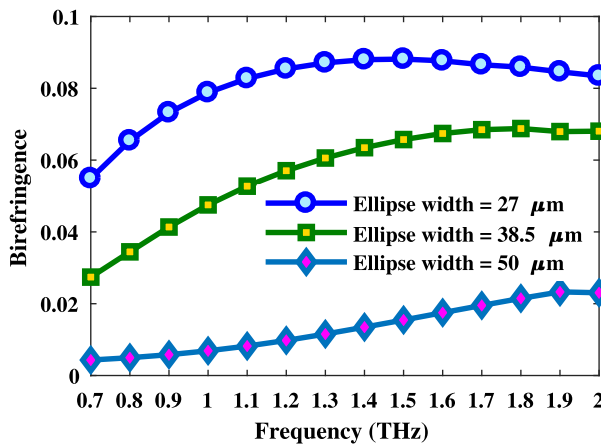


Fig. 5. Birefringence vs frequency at optimal D_{core} , $d = 4 \mu\text{m}$, and different W values.

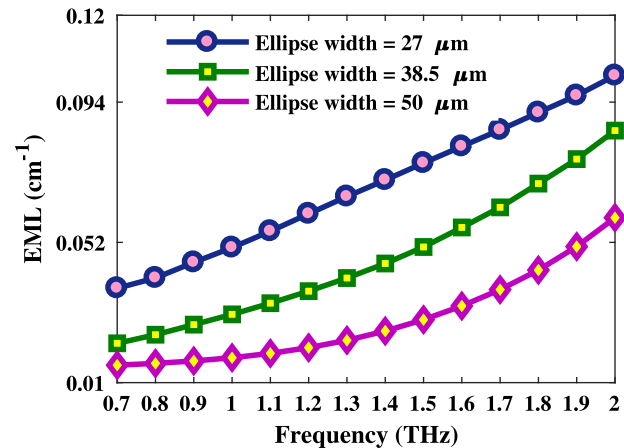


Fig. 7. EML vs frequency at different W with other optimum design parameters.

Now, in order to choose optimum major axis lengths and strut width we characterize the fiber with reduced major axis length than the maximum and increased strut width. At optimal D_{core} and $d = 4 \mu\text{m}$ we changed the major axis length of elliptical air holes to $L = 0.43D_{core}$, $L_1 = 0.26D_{core}$ and characterizes the birefringence and EML as shown in Fig. 6. We find that reducing the major axis lengths from its maximum value reduces the birefringence and at the same time increase the EML in a large scale. Therefore, we choose $L = 0.49D_{core}$ and $L_1 = 0.32D_{core}$ as optimal major axis length of the elliptical air holes placed inside the core of the fiber.

Now, keeping D_{core} , L and L_1 optimum we increased the strut width to $4 \mu\text{m}$ and set d as $d = 8 \mu\text{m}$ and characterizes the birefringence and EML accordingly that is shown in Fig. 6. We can see that increase of strut width reduces the birefringence and increases the EML. This is because increases strut width increases the material into the fiber that reduces the index difference between core and cladding and increases the EML. The impact of strut width of the fiber can be observed by comparing Figs. 5 and 7 with Fig. 6. Therefore, considering the characteristics of birefringence and EML we choose $d = 4 \mu\text{m}$ as the optimum design parameter.

The characteristic of EML with respect to frequency at different W value is shown in Fig. 7. It is clearly seen that EML increases with frequency. From the empirical equation $\alpha(\nu) = \nu^2 + 0.63\nu - 0.13$, dB/cm [29] of calculating material absorption loss it can be validated that EML increases linearly with frequency. It is also observed that EML reduces with the increase of W . Increases of W reduces the amount of material inside the core region and thus the amount of EML reduces.

Fig. 7 indicates that at $W = 0.143D_{core}$ the EML is lower than $W = 0.11D_{core}$ and $W = 0.077D_{core}$. However, we choose $W = 0.077D_{core}$

as optimum as our main concern is the property of birefringence. Birefringence mainly depends on the asymmetry between the x and y polarization mode. At lower W the difference between the orthogonal polarization modes increases which consequently increases the birefringence. We could reduce the value of W further than $W = 0.077D_{core}$ to increase the birefringence but that would increase the EML too. Therefore, this is another reason for choosing $W = 0.077D_{core}$ as optimum.

The confinement loss as a function of frequency at orthogonal polarization modes and other optimal design conditions is shown in Fig. 8. It can be seen that confinement loss decreases with the increase of frequency. This is because with frequency increase more light starts to constrict strictly in the porous core region [30].

Here, we choose 1 THz as optimum frequency because at 1 THz the obtained birefringence is 0.079, the obtained EML is 0.05 cm^{-1} which are better than the previously proposed [36,37,31,38,39] optical waveguides. Moreover the obtained confinement loss at 1 THz is $7.24 \times 10^{-7} \text{ cm}^{-1}$ that is negligible that compared to the obtained EML. At lower values than 1 THz we can see that the EML is lower but at the same time the birefringence is lower and the confinement loss is higher. We could also choose higher values than 1 THz as optimum to get high birefringence but that also increases the EML. Therefore, considering birefringence, EML and confinement loss property we choose 1 THz as the optimum design condition.

The characteristics of dispersion with respect to frequency at different polarization is shown in Fig. 9. It can be observed that, for the x and y polarization mode the dispersion variation within the frequency of operation (0.7–2.0 THz) is $0.80 \pm 0.25 \text{ ps/THz/cm}$ and $0.62 \pm 0.17 \text{ ps/THz/cm}$ respectively. However, we choose 0.8–1.7 THz

Table 1
Comparison between birefringence, dispersion, EML and confinement loss of the proposed PCF with other PCFs discussed in the literature.

Ref.	Bulk material	B	β_2 (ps/THz/cm)	α_{eff} (cm ⁻¹)	L_c (cm ⁻¹)
[31]	Topas	0.03	0.2 – 1	0.06	0.0004
[32]	Topas	0.026	–	0.04	–
[34]	Topas	0.075	1.25 ± 0.5	0.07	1.302
[35]	Topas	0.033	–	0.09	10 ^{-3.8}
[36]	Topas	0.0483	0.51	0.085	0.008
[37]	Topas	0.045	0.9 ± 0.26	0.08	–
[38]	Topas	0.01	0 – 1.5	0.04	0.0004
[39]	Topas	0.0119	–	0.0689	–
This manuscript	Zeonex	0.079	0.49 ± 0.05	0.05	7.24 × 10 ⁻⁷

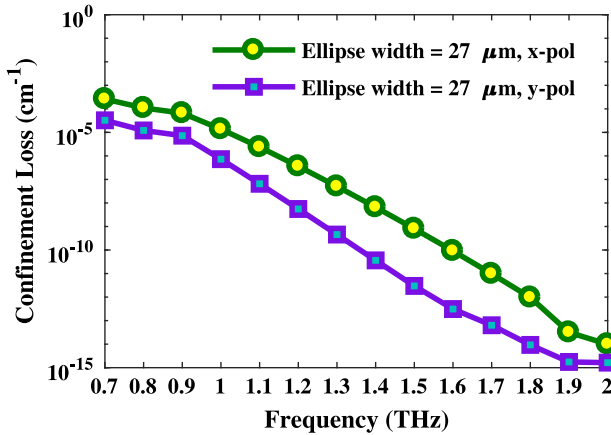


Fig. 8. Confinement loss vs frequency at orthogonal polarization mode with other optimum design conditions.

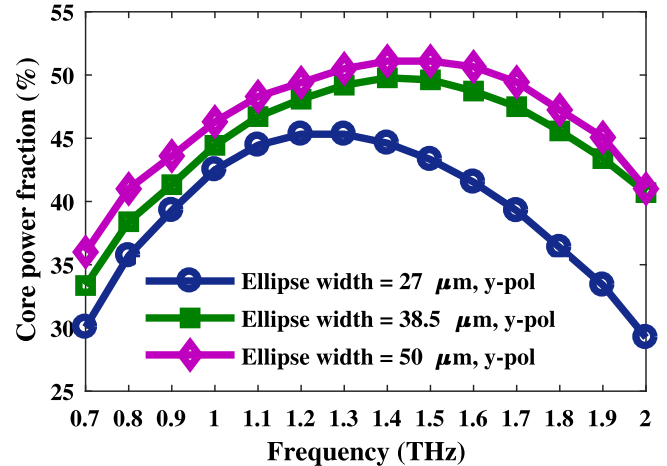


Fig. 10. Core power fraction vs frequency at optimum design conditions.

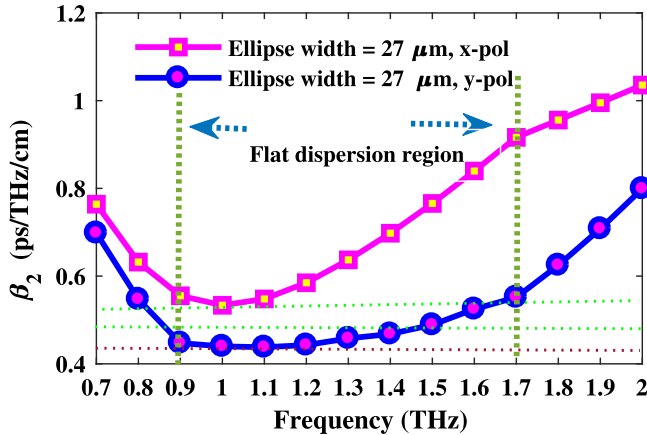


Fig. 9. Dispersion vs frequency at different polarization modes and other optimum design conditions.

as the optimum frequency of operation because within this range the obtained value of dispersion is 0.49 ± 0.05 ps/THz/cm that is almost zero and variation is negligible. The reason of obtaining near zero and flattened dispersion is the use of Zeonex as the background material as well as compact kagome structure with simple core structure. Note that Zeonex has a negligible material dispersion therefore we only calculated the waveguide dispersion which mostly depends on the geometrical structure of the waveguide [44–46,53,54]. To our knowledge, the obtained dispersion is very low with negligible flatness that might be suitable for multichannel communication application of terahertz waves.

The amount of useful power transmitted through the core at different W is shown in Fig. 10. It can be observed that core power fraction

increases with the increase of W . Increasing of W means increasing the length of minor axis of elliptical air holes that causes more power to be transmitted through it. It is also observed that, the core power fraction increases from 0.7–1.4 THz and then starts to decrease at higher frequencies. This is because at 1.4 THz the confinement of light through the core reaches its optimum point and further increase of frequency starts to increase transmission through the cladding as well as material region. At optimum design conditions the obtained core power fraction is 44%.

The modal effective area as a function of frequency at optimum design conditions with different polarization mode is shown through Fig. 11. It is observed that, modal effective area decreases with frequency. The amount of light confined in the core area decreases when the frequency increases and thus the phenomenon happened. At optimum design parameters the obtained effective area is $0.95 \times 10^5 \mu\text{m}^2$.

The characteristics comparison of the proposed oligo-porous core PCF with other terahertz PCF is shown in Table 1. It clearly indicates that, beside simplicity in core structure the oligo-porous core structure shows improved characteristics over prior PCFs.

4. Conclusion

A novel photonic crystal fiber consisting of kagome lattice and elliptical air holes inside the core is proposed and analyzed for the terahertz frequency band. Simulation results reveal that, an ultra high birefringence of 0.079, lower effective material loss of 0.05 cm^{-1} and negligible confinement loss of $7.24 \times 10^{-7} \text{ cm}^{-1}$ is obtained at 1 THz frequency. Furthermore, the PCF displays a low near zero dispersion flattened characteristic of 0.49 ± 0.05 ps/THz/cm over a wide bandwidth, a moderate core power fraction of 44% and high modal effective area of $0.95 \times 10^5 \mu\text{m}^2$. Moreover, the proposed PCF can

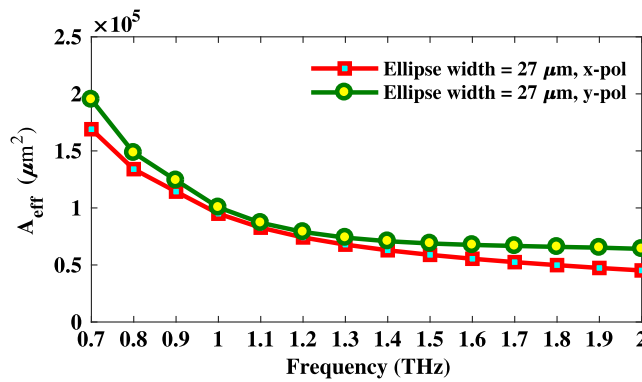


Fig. 11. Effective area vs frequency at optimum design conditions.

easily be engineered with the state of the art fabrication technology. Thus, it can be anticipated that the proposed PCF can be applicable in polarized terahertz filters, sensors, multichannel communications and polarization maintaining terahertz wave guidance.

Acknowledgment

Funding information

Funding from the Australian Research Council (DP170104984) is gratefully acknowledged.

References

- [1] D. Abbott, X.C. Zhang, Scanning the issue: T-ray imaging, sensing, and refection, *Proc. IEEE* 95 (8) (2007) 1509–1513.
- [2] W. Withayachumnankul, G.M. Png, X. Yin, S. Atakaramians, I. Jones, H. Lin, B.S.Y. Ung, J. Balakrishnan, B.W.-H. Ng, B. Ferguson, S.P. Mickan, B.M. Fischer, D. Abbott, T-ray sensing and imaging, *Proc. IEEE* 95 (8) (2007) 1528–1558.
- [3] M.S. Islam, J. Sultana, K. Ahmed, A. Dinovitsner, M.R. Islam, B.W.-H. Ng, D. Abbott, A novel approach for spectroscopic chemical identification using photonic crystal fiber in the Terahertz Regime, *IEEE Sens. J.* (2017). <http://dx.doi.org/10.1109/JSEN.2017.2775642>.
- [4] C.J. Strachan, P.F. Taday, D.A. Newnham, Using terahertz pulsed spectroscopy to quantify pharmaceutical polymorphism and crystallinity, *J. Pharm. Sci.* 94 (4) (2005) 837–846.
- [5] J.Q. Zhang, D. Grischkowsky, Waveguide terahertz time-domain spectroscopy of nanometer water layers, *Opt. Lett.* 29 (14) (2004) 1617–1619.
- [6] W. Withayachumnankul Engineering aspects of terahertz time-domain spectroscopy (Ph.D Thesis), The University of Adelaide, 2009.
- [7] J. Balakrishnan, B.M. Fischer, D. Abbott, Sensing the hygroscopicity of polymer and copolymer materials using terahertz time-domain spectroscopy, *Appl. Opt.* 48 (12) (2009) 2262–2266.
- [8] R.M. Woodward, V.P. Wallace, D.D. Arnone, Terahertz pulsed imaging of skin cancer in the time and frequency domain, *J. Biol. Phys.* 29 (2) (2003) 257–261.
- [9] M. Nagel, P.H. Bolivar, M. Brucherseifer, H. Kurz, A. Bosserhoff, R. Btner, Integrated THz technology for label-free genetic diagnostics, *Appl. Phys. Lett.* 80 (54) (2002) 154–156.
- [10] H. Bao, K. Nielse, H. Rasmussen, P. Jepsen, O. Bang, Design and optimization of mechanically down-doped terahertz fiber directional couplers, *Opt. Express* 22 (8) (2014) 9486–9497.
- [11] S. Li, H. Zhang, Y. Hou, J. Bai, W. Liu, S. Chang, Terahertz polarization splitter based on orthogonal microstructure dual-core photonic crystal fiber, *Appl. Opt.* 52 (14) (2013) 3305–3310.
- [12] W. Yuan, L. Khan, D.J. Webb, K. Kalli, H.K. Rasmussen, A. Stefani, O. Bang, Humidity insensitive TOPAS polymer fiber Bragg grating sensor, *Opt. Express* 19 (20) (2011) 19731–19739.
- [13] C. Markos, A. Stefani, K. Nielsen, H.K. Rasmussen, W. Yuan, O. Bang, High- T_g TOPAS microstructured polymer optical fiber for fiber Bragg grating strain sensing at 110 degrees, *Opt. Express* 21 (4) (2013) 4758–4785.
- [14] R. Kersting, G. Strasser, K. Unterrainer, Terahertz phase modulator, *Electron Lett.* 36 (13) (2000) 1156–1158.
- [15] W.L. Chan, H.T. Chen, A.J. Taylor, I. Brener, M.J. Cich, D.M. Mittleman, A spatial light modulator for terahertz beams, *Appl. Phys. Lett.* 94 (21) (2009) 213511–213513.
- [16] B.S. Williams, Terahertz quantum-cascade lasers, *Nature Photon.* 1 (2007) 517–525.
- [17] R.W. McGowan, G. Gallot, D. Grischkowsky, Propagation of ultrawideband short pulses of terahertz radiation through sub-millimeter-diameter circular waveguides, *Opt. Lett.* 24 (20) (1999) 1431–1433.
- [18] G. Gallot, S.P. Jamison, R.W. McGowan, D. Grischkowsky, Terahertz waveguides, *J. Opt. Soc. Am. B.* 17 (5) (2000) 851–863.
- [19] R. Mendis, D. Grischkowsky, Undistorted guided-wave propagation of subpicosecond terahertz pulses, *Opt. Lett.* 26 (11) (2001) 846–848.
- [20] M. Wächter, M. Nagel, H. Kurz, Frequency-dependent characterization of THz Sommerfeld wave propagation on single-wires, *Opt. Express* 13 (26) (2005) 10815–10822.
- [21] M. Wächter, M. Nagel, H. Kurz, Metallic slit waveguide for dispersion-free low-loss terahertz signal transmission, *Appl. Phys. Lett.* 90 (6) (2007) 061111.
- [22] J. Sanghera, I. Aggarwal, *Infrared Fiber Optics*, CRC Press, Boca Raton, FL, 1998.
- [23] P. France, M.G. Drexhage, J.M. Parker, M.W. Moore, S.F. Carter, J.V. Wright, *Fluoride Glass Optical Fibres*, Blackie, London, 1990.
- [24] I. Agarwal, G. Lu, *Fluoride Glass Optical Fiber*, Academic Press, New York, 1991.
- [25] T. Katsuyama, H. Matsumura, *Infrared Optical Fibers*, Adam Hilger, Bristol, 1989.
- [26] G.K.M. Hasanuzzaman, M.S. Habib, S.M.A. Razzak, M.A. Hossain, Y. Namihira, Low loss single mode porous-core Kagome Photonic crystal fiber for THz wave guidance, *J. Light-Wave Technol.* 33 (19) (2015) 15400618.
- [27] M.S. Islam, S. Rana, M.R. Islam, M. Faisal, H. Rahman, J. Sultana, Porous core photonic crystal fiber for ultra-low material loss in THz regime, *IET Commun.* 10 (16) (2016) 2179–2183.
- [28] S. Islam, M.R. Islam, M. Faisal, A.S.M.S. Arefin, H. Rahman, J. Sultana, S. Rana, Extremely low-loss, dispersion flattened porous-core photonic crystal fiber for terahertz regime, *Opt. Eng.* 55 (7) (2016) 076117.
- [29] M.S. Islam, J. Sultana, S. Rana, M.R. Islam, M. Faisal, S.F. Kaijage, D. Abbott, Extremely low material loss and dispersion flattened TOPAS based circular porous fiber for long distance terahertz wave transmission, *Optical Fiber Technol.* 24 (2016) 6–11.
- [30] M.S. Islam, J. Sultana, J. Atai, D. Abbott, S. Rana, M.R. Islam, Ultra low loss hybrid core porous fiber for broadband applications, *Appl. Opt.* 56 (9) (2017) 1232–1237.
- [31] Z. Wu, Z. Shi, H. Xia, X. Zhou, Q. Deng, J. Huang, X. Jiang, W. Wu, Design of highly birefringent and low-loss oligoporous-core THz Photonic crystal fiber with single circular air-hole unit, *IEEE Photonics J.* 8 (6) (2016) 4502711.
- [32] S. Atakaramians, V. Afshar, B.M. Fischer, D. Abbott, T.M. Monro, Low loss, low dispersion and highly birefringent terahertz porous fibers, *Opt. Commun.* 282 (1) (2008) 36–38.
- [33] D. Chen, H.Y. Tam, Highly Birefringent Terahertz fibers based on super-cell structure, *J. Lightwave Technol.* 28 (12) (2010) 1858–1863.
- [34] R. Islam, M.S. Habib, G.K.M. Hasanuzzaman, R. Ahmad, S. Rana, S.F. Kaijage, Extremely high-birefringent asymmetric slotted-core photonic crystal fiber in THz regime, *IEEE Photon. Technol. Lett.* 27 (21) (2015) 2222–2225.
- [35] G.K.M. Hasanuzzaman, S. Rana, M.S. Habib, A novel low loss, highly birefringent photonic crystal fiber in THz regime, *IEEE Photon. Technol. Lett.* 28 (8) (2016) 899–902.
- [36] M.R. Hasan, M.S. Anower, M.A. Islam, S.M.A. Razzak, Polarization-maintaining low-loss porous-core spiral photonic crystal fiber for terahertz wave guidance, *Appl. Opt.* 55 (15) (2016) 4145–4152.
- [37] R. Islam, M.S. Habib, G.K.M. Hasanuzzaman, S. Rana, A. Sadat, Novel porous fiber based on dual-asymmetry for low-loss polarization maintaining THz wave guidance, *Opt. Express* 41 (3) (2016) 440–443.
- [38] Z. Wu, X. Zhou, H. Xia, Z. Shi, J. Huang, X. Jiang, W. Wu, Low-loss polarization-maintaining THz photonic crystal fiber with a triple-hole core, *Appl. Opt.* 56 (8) (2017) 2288–2293.
- [39] K. Ahmed, S. Chowdhury, B.K. Paul, M.S. Islam, S. Sen, M.I. Islam, S. Asaduzzaman, Ultrahigh birefringence, ultralow material loss porous core single-mode fiber for terahertz wave guidance, *Appl. Opt.* 56 (12) (2017) 3477–3483.
- [40] Y.Y. Wang, N.V. Wheeler, F. Couny, P.J. Roberts, F. Benabid, Low loss broadband transmission in hypocycloid-core Kagome hollow-core photonic crystal fiber, *Opt. Lett.* 36 (5) (2011) 669–671.
- [41] M.R. Hasan, S. Akter, T. Khatun, A.A. Rifat, M.S. Anower, Dual-hole unit-based kagome lattice microstructure fiber for low-loss and highly birefringent terahertz guidance, *Opt. Eng.* 56 (4) (2017) 043108.
- [42] J. Yang, J. Zhao, C. Gong, H. Tian, L. Sun, P. Chen, L. Lin, Weiwei Liu, 3D printed low-loss THz waveguide based on Kagome photonic crystal structure, *Opt. Express* 24 (30) (2016) 22455.
- [43] A. Hossain, Y. Namihira, Light source design using Kagome lattice hollow core photonic crystal fibers, *Opt. Rev.* 21 (5) (2014) 490–495. <https://www.zeonex.com>.
- [44] J. Anthony, R. Leonhardt, A. Argyros, M.C.J. Large, Characterization of a microstructured Zeonex terahertz fiber, *J. Opt. Soc. Amer. B* 28 (5) (2011) 1013–1018.
- [45] G. Woyessa, A. Fasano, C. Markos, A. Stefani, H.K. Rasmussen, O. Bang, Zeonex microstructured polymer optical fiber: Fabrication friendly fibers for high temperature and humidity insensitive Bragg grating sensing, *Opt. Mater. Express* 7 (1) (2017) 286–295.
- [46] Fabrications of Photonic Crystal Fibers, *Photonic Crystal Fibre Science*, accessed on 19th June, 2017 [Online]. Available: <http://www.mpl.mpg.de/en/russell/research/topics/fabrication.html>.

- [48] H. Ebendorff-Heidepriem, T.M. Monro, Extrusion of complex preforms for microstructured optical fibers, *Opt. Express* 15 (23) (2007) 15086–15092.
- [49] S. Atakaramians, S. Afshar, H. Ebendorff-Heidepriem, M. Nagel, B.M. Fischer, D. Abbott, T.M. Monro, THz porous fibers: Design, fabrication and experimental characterization, *Opt. Express* 17 (16) (2009) 14053–14062.
- [50] N.A. Issa, M.A.V. Eijkelenborg, M. Fellew, F. Cox, G. Henry, M.C.J. Large, Fabrication and study of microstructured optical fibers with elliptical holes, *Opt. Lett.* 29 (12) (2004) 1336–1338.
- [51] F. Liu, H. Gao, Q. Xu, Y. Zhang, Fabrication and characteristics of elliptical-holes and near elliptical core hexangular lattice photonic crystal fibers based on polymer, *Advanced Materials Research* 279 (2011) 151–156.
- [52] Y. Ruan, H. Ebendorff-Heidepriem, S. Afshar, T.M. Monro, Light confinement within nano-holes in nanostructured optical fibers, *Opt. Express* 18 (25) (2010) 26018–26026.
- [53] N. Sultanova, S. Kasarova, I. Nikolov, Dispersion properties of optical polymers, *Acta Phys. Polonica A* 116 (4) (2009) 585.
- [54] J. Anthony, R. Leonhardt, A. Argyros, M.C.J. Large, Characterization of a microstructured Zeonex terahertz fiber, *J. Opt. Soc. Amer. B* 28 (5) (2011) 1013–1018.